Georgia Tech Space Systems Design Laboratory

An Orbital Capability Analysis of CubeSats Utilizing a Bimodal Monopropellant Propulsion System

AE 8900 Special Problems Report

Author: William R. Blair
Advisor: Dr. E. Glenn Lightsey

Space Systems Design Lab
Daniel Guggenheim School of Aerospace Engineering
Georgia Institute of Technology
July 30th, 2021

An Orbital Capability Analysis of CubeSats Utilizing a Bimodal Monopropellant Propulsion System

William R. Blair[1] and E. Glenn Lightsey[2]
Georgia Institute of Technology, Atlanta, Georgia, 30313

The Space Systems Design Lab at Georgia Institute of Technology has performed extensive research in the development and integration of green monopropellant systems for small satellites, culminating in the design and assembly of the propulsion system for Lunar Flashlight (LFPS) [3]. The Spectre bimodal propellant system seeks to take the benefits of the LFPS and couple it with an electrospray propulsion system, giving the spacecraft capability to perform high-thrust maneuvers using standard chemical propulsion methods, and to perform efficient, low-thrust maneuvers using the electrospray system [2]. To assist with this design process, a simulation framework was developed in MATLAB to model the dynamics of the spacecraft as well as to determine logic and methods for mission planning. To this end, the vehicles motion was characterized and a performance baseline was established for various orbital maneuvers and mission designs. The development of this simulation, as well as challenges and future work, is discussed herein.

I. Nomenclature

$\bar{r}$	=	Position vector
$\dot{\bar{r}}$	=	Velocity vector
$\ddot{\bar{r}}$	=	Acceleration vector
μ	=	Earth Gravitational constant
$\bar{F}$	=	Force vector
m	=	Vehicle mass
$\bar{X}$	=	Attitude matrix
$\bar{x}$	=	x-axis matrix for attitude representation
$\bar{y}$	=	y-axis matrix for attitude representation
$\bar{z}$	=	z-axis matrix for attitude representation
ECI	=	Earth Centered Inertial Frame
LVLH	=	Local Vertical, Local Horizontal Frame
ϕ	=	Roll Euler Angle
Θ	=	Pitch Euler Angle
ψ	=	Yaw Euler Angle
$\bar{u}$	=	Spacecraft pointing vector
$\dot{m}$	=	Mass flow rate
Isp	=	Specific Impulse
g_0	=	Gravitational acceleration
ΔV	=	Velocity Change

II. Spectre Propulsion System

Bimodal propulsion is the next step for green, small satellite propulsion systems and can offer significant capability in a small package. The Spectre propulsion system combines a chemical propulsion unit, developed by the Georgia Tech Space Systems Design Lab, with an electrospray system developed by the Massachusetts Institute of

[1] Graduate Student and Research Engineer, Georgia Tech Research Institute, reilly.blair@gtri.gatech.edu
[2] Professor, Guggenheim School of Aerospace Engineering, glenn.lightsey@gatech.edu

Technology. Given that both systems are powered by the same monopropellant fuel (AF-M315E), the need for multiple propellant tanks and associated systems is avoided. The combination of these systems offers the capability to perform high thrust maneuvers and high efficiency maneuvers while minimizing size and weight. The versatility offered by this system has the potential to enable mission profiles reserved for larger spacecraft, such as: LEO to GEO trajectories, GEO to Lunar trajectories, interplanetary missions, or mission profiles requiring precise station-keeping.

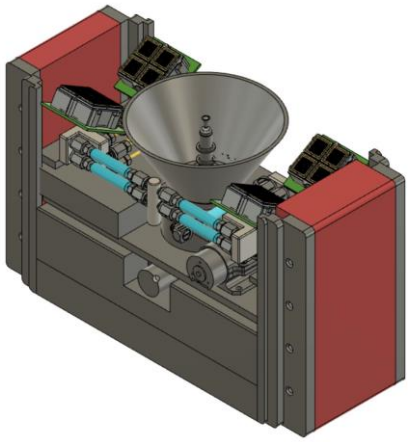

Figure 1: Spectre Propulsion System

The initial design of the Spectre system utilizes a 1 Newton Chemical Thruster and a configuration of 4 Electrospray units totaling 15 μN of thrust. This system is packaged in a 3.5U – 4U form-factor and is intended to be installed on a 12U sized satellite. A model of the system is shown above in Figure 1 while Figures 2 and 3 display the electrospray and chemical systems, respectively. Performance specifications for the propulsion systems are listed below in Table 1.

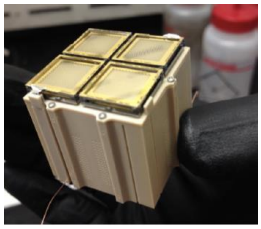

Figure 2: Electrospray Thruster

Figure 3: Chemical Thruster

Table 1: Propulsion Component Specifications

Characteristic	Value
Chemical Thrust	1 N
Chemical Specific Impulse	250 sec
Electrospray Thrust	15 μN
Electrospray Specific Impulse	1200 sec

The initial configuration that will be explored is shown above, with the potential for other analyses using larger form-factors and other chemical thruster sizes. Current designs for different sized vehicles and their associated weights can be seen below in Table 2.

Table 2: Spectre Sizing Configurations

Vehicle Size	6U	12U	27U
Propellant Mass (kg)	2.94	4.96	9.55
Total Mass (kg)	8	12	30

Plasma Processes, the developer of the chemical thruster, has designed thrusters ranging from 100mN up to 100 N. The use of more powerful thrusters could be explored in further excursions, but will require tradeoffs such as efficiency or weight that are not currently characterized for vehicle integration.

III. Simulation Framework

An initial simulation framework was established in MATLAB to model Six Degree-of-Freedom (6DOF) vehicle dynamics utilizing an ODE45 integrator. In order to evaluate the performance of the Spectre propulsion system, this analysis primarily focused on the kinematics of the spacecraft and assumed attitude control will be provided via another system.

A basic flow of the simulation framework can be seen below in Figure 4. Initial setup of the spacecraft's parameters occurs outside of the integration loop. This includes selecting the thruster to test, selecting the mission profile (Constant Burn, Orbit Raising at Apogee and Perigee, Orbital Plane change, etc.), and establishing the initial orbital elements of the vehicle. These parameters are stored inside a global structure, with some being updated at each time-step. This comes at a performance cost, but streamlines the process and reduces clutter in the simulation.

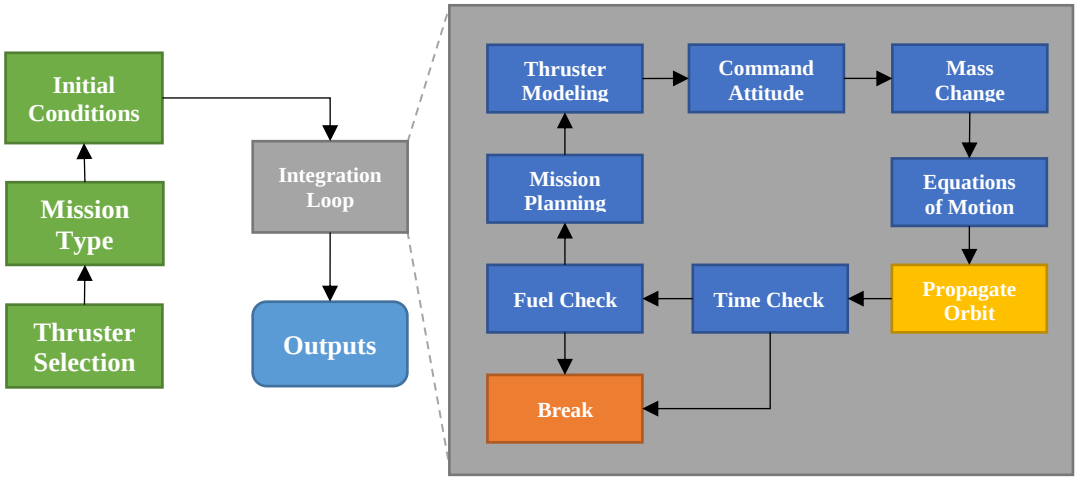

Figure 4: Simulation Block Diagram

A. Integration and Orbit Propagation

One major challenge encountered was the choice of integrator to use for the propagation of the vehicle. MATLAB has excellent built-in integrators, such as ODE45, that allow for rapid and efficient integration of ordinary differential equations. These stock equations are simple to implement, but it soon became apparent that there were flaws in the application to this specific problem, namely when it came to the highly non-linear integration time-step. This became a significant issue when attempting to determine the length of time the thruster had been activated, which cascaded into issues with the changing fuel of the spacecraft. The non-linearity was reflected in issues around the boundaries of the "windows" for thruster activation, namely that thruster state would vacillate between on and off, causing issues with the logic used for fuel reduction. This was able to be bypassed by performing a "double looped" setup, using a fixed time-step on the exterior loop and the standard ODE45 integrator on the inside loop. This came at a large computational cost and was unacceptable as a potential solution.

This lead to the development of a custom Runga-Kutta 44 (RK44) integrator with a fixed time-step, using the methodology shown below in Equations 1-5.

$$k_1 = \mathrm{f}_{orbit}(\mathrm{X}, \mathrm{F}_{Thrust}) \tag{1}$$

$$k_2 = \mathrm{f}_{orbit}(\mathrm{X} + k_1 * \frac{h}{2}, \mathrm{F}_{Thrust}) \tag{2}$$

$$k_3 = \mathrm{f}_{orbit}(\mathrm{X} + k_2 * \frac{h}{2}, \mathrm{F}_{Thrust}) \tag{3}$$

$$k_4 = \mathrm{f}_{orbit}(\mathrm{X} + k_3, \mathrm{F}_{Thrust}) \tag{4}$$

$$X = X + \frac{h}{6} * (k_1 + 2 * k_2 + 2 * k_3 + k_4) \tag{5}$$

Where X is the vehicle state vector, the *k*'s are integration constants, *h* is the time-step, F is the force vector from the thruster, and f_{orbit} is the orbital dynamics function. This method offered relatively efficient integration as well as a fixed time-step that allowed for simple logic checks for thruster activation and fuel loss.

Once passed into the integration loop, the mission begins with logic checks performed based off of established mission plans to determine the status of the spacecraft's thruster as well as the orientation of the vehicle. The interactions and specifics of each of these subsystems is detailed throughout the next sections.

B. Equations of Motion

The following equations of motion are used to characterize the dynamics of the vehicle inside the integration loop. This began with the standard equation for a point mass orbiting a much larger body, as shown in Equation 6.

$$\ddot{\bar{r}}_{Gravity} = -\frac{\mu}{r^3} * \bar{r} \tag{6}$$

Where $\bar{r}$ is the vehicles position, $\ddot{\bar{r}}_{Gravity}$ is the acceleration on the vehicle from gravity, and μ is the gravitational constant for Earth. Next, it was necessary to model the force that the propulsion system imposes on the vehicle. This process is detailed using the basic F = ma relationship as shown in Equation 7. With m being vehicle mass, $\bar{F}_{Thrust}$ is the force imposed by the propulsion system and $\ddot{\bar{r}}_{Propulsion}$ is the acceleration on the vehicle from the propulsion system.

$$\ddot{\bar{r}}_{Propulsion} = \frac{\bar{F}_{Thrust}}{m} \tag{7}$$

These accelerations are then summed to determine the total acceleration on the vehicle from both gravity and propulsion. The resulting equation of motion below describes the vehicle's motion in terms of both the gravitational force and thruster force.

$$\ddot{\bar{r}}_{Vehicle} = \ddot{\bar{r}}_{Gravity} + \ddot{\bar{r}}_{Propulsion} \tag{8}$$

$$\ddot{\bar{r}}_{Vehicle} = -\frac{\mu}{r^3} * \bar{r} + \frac{\bar{F}_{Thrust}}{m} \tag{9}$$

C. Coordinate Frames and Spacecraft Orientation

The two reference frames utilized in this analysis are the Earth Centered Earth Fixed (ECEF) frame for the orbital propagation and the Local Vertical Local Horizontal (LVLH) frame for commanding the attitude of the vehicle. The ECEF frame reduces the complexity of the simulation by disregarding the rotational motion of the earth. The LVLH frame is commonly utilized for attitude representations of spacecraft. It should be noted that the ECEF frame is the primary frame of reference for the simulation, with the LVLH frame only being used for commanding the attitude of the spacecraft when required. A notional sketch of the spacecraft orientation is shown below in Figure 5.

In the LVLH frame, the x-axis points along the velocity vector frame, while the z-axis is nadir pointing. Using this information, a transformation between ECEF and LVLH can be calculated via Equations 10 through 14.

$$\bar{X}_{ECI} = \begin{bmatrix} \bar{x}_{ECEF} \\ \bar{y}_{ECEF} \\ \bar{z}_{ECEF} \end{bmatrix} = \begin{bmatrix} 1 & 0 & 0 \\ 0 & 1 & 0 \\ 0 & 0 & 1 \end{bmatrix} \tag{10}$$

$$\bar{X}_{LVLH} = \begin{bmatrix} \bar{x}_{LVLH} \\ \bar{y}_{LVLH} \\ \bar{z}_{LVLH} \end{bmatrix} = \begin{bmatrix} \frac{\dot{\bar{r}}_{ECEF}}{|\dot{\bar{r}}_{ECEF}|} \\ \frac{-\bar{r}_{ECEF}}{|\bar{r}_{ECEF}|} \\ \bar{z}_{LVLH} \times \bar{x}_{LVLH} \end{bmatrix} \tag{11}$$

$$R_{LVLV2ECI} = [\bar{x}_{LVLH} \quad \bar{y}_{LVLH} \quad \bar{z}_{LVLH}] \tag{12}$$

Using this transformation, the direction of the spacecraft can be commanded using Roll-Pitch-Yaw notation such that:

$$\bar{u}_{LVLH} = \begin{bmatrix} C\psi C\vartheta & C\psi S\vartheta S\phi - S\psi C\phi & C\psi S\Theta C\phi + S\psi S\phi \\ S\psi C\vartheta & S\psi S\Theta S\phi + C\psi C\phi & S\psi S\Theta C\phi - C\psi S\phi \\ -S\vartheta & C\Theta S\phi & C\Theta C\phi \end{bmatrix} \begin{bmatrix} 1 \\ 0 \\ 0 \end{bmatrix} \tag{13}$$

$$\bar{u}_{ECI} = R_{LVLV2ECEF} * \bar{u}_{LVLH} \tag{14}$$

Where $\bar{u}_{LVLH}$ is the direction that the spacecraft is pointing in the LVLH frame, *C* and *S* are the cosine and sine functions, ϕ is the roll angle, Θ is the pitch angle and ψ is the yaw angle.

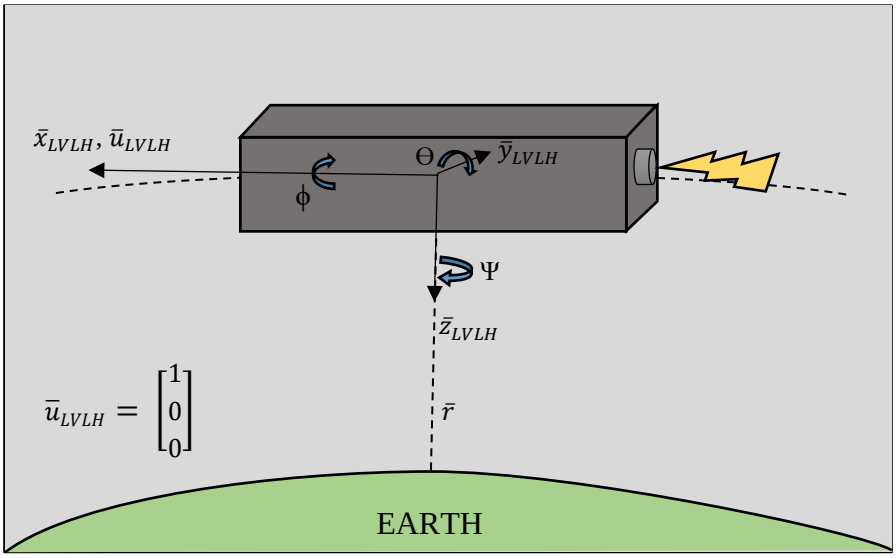

Figure 5: Notional Spacecraft Orientation (LVLH Frame)

D. Thruster Modeling and Logic

Outside of the equations of motion, the primary area of interest is the force impacted upon the vehicle by the chemical and electrospray thruster. Basic methods of modeling delta V on a spacecraft, namely the Tsiolkovsky rocket equation (shown in Equation 15), offer simplistic ways of capturing the capability of a propulsion system, but the assumption of instantaneous impulse fails to capture important vehicle characteristics. Primarily, this is the mass change of the spacecraft due to the ejection of fuel at each integration time-step. This gap is rectified by decomposing the thruster into its mass flow rate and accounting for that change on the spacecraft over time.

$$\Delta V = Isp * g_0 \ln(\frac{m_0}{m_f}) \tag{15}$$

These propulsion systems can both be modeled using the same methodology, so the technical approach below applies for both systems. Using the equations below, the mass flow rate of the propulsion system can be determined (Assumption: there is not throttle capability on the system. The system is either fully ON or OFF). This mass flow rate is used to account for propellant mass loss as the spacecraft performs burns. The mass change of the spacecraft is updated at each simulation time-step.

$$\dot{m}_{prop} = \frac{F_{Thrust}}{Isp * g_0} \tag{16}$$

Where $\dot{m}_{prop}$ is the mass flow rate of the propellant, F_{Thrust} is the scalar force due to the thruster, Isp is the specific impulse and g_0 is gravity.

Additionally, the direction of this force will need to be transformed to be in-line with the direction of the spacecraft. Initial simulations will assume spacecraft orientation is parallel with respect to the spacecraft velocity vector (ie: tangential to the orbital ellipse at all times). This assumes that the spacecraft has attitude control to maintain said orientation. This is done by acquiring the pointing vector in the ECEF frame and multiplying by the thruster force as shown in Equation 17.

$$\bar{F}_{Thrust} = F_{Thrust} * \bar{u}_{ECEF} \tag{17}$$

IV. Performance Analysis

A. Constant Burn Orbit Raising

Initial simulations focused on a 6U CubeSat pointing along the velocity vector. This orientation is optimal for raising the orbit of the satellite and can offer insight into the basic capability of the vehicle. The simulation was meant to model a CubeSat deployed from the orbit of the ISS. This was simplified to a circular orbit with an altitude of 418 kilometers and an inclination of around 50°. Initial mission planning involved utilizing a constant burn until fuel depletion to determine orbit raising capability using minimal mission planning.

It should also be noted that given the extremely low mass-flow rate of the electrospray system, coupled with the size of the fuel available onboard, it would take an extremely long duration to expend all available fuel utilizing only the electrospray thrusters. Initial calculations came out to 71 years to expend 2.3 kg of fuel. It was initially planned to analyze the orbital raising capabilities of solely using each subsystem, but given the infeasible timeframe of an electrospray-only mission, that approach needed to be re-examined. Results from a chemical-only constant burn are displayed in Table 3.

Table 3: Chemical Only - Constant Burn

Size	ΔV (km/s)	Altitude Gain (km)	Maneuver Time (hrs)
6U	1.138	2155	1.56
12U	1.411	2756	2.70
27U	1.104	2246	6.46

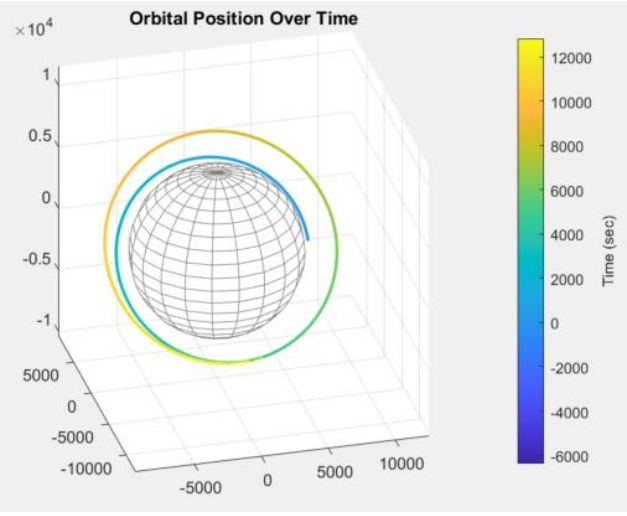

Figure 6: Constant Burn Orbit Raising

A quick verification was performed using the Tsiolkovsky rocket equation to ensure these values are within the realm of feasibility. Table 4 displays the results of this analysis.

Table 4: Delta V Variation for Constant Burn

Size	ΔV (Sim)	ΔV (Rocket Eqn)	% Difference
6U	1.138	0.830	27%
12U	1.411	0.983	30.3%
27U	1.104	0.716	35.1%

This difference is non-trivial and requires further investigation to ensure validity. These differences could arise from multiple sources or could be a combination of inherent modeling difference and potential issues with the thruster modeling methodology.

B. Apogee / Perigee Orbit Raising

The previous brute force method of raising the orbit seemed unlikely to be representative of potential real-world scenarios of spacecraft use, so the next step was to impose mission planning logic into the simulation to ensure burns were conducted at the most efficient orbital positions. In this case, raising an orbit involved firing at perigee to raise your apogee altitude. This effectively creates an elliptical orbit that then needs to be circularized with a second burn.

The method utilized in this simulation schedules the orbit-raising burns as a function of the spacecraft's true anomaly. Given that firing the spacecraft exactly at perigee and apogee requires near-instantaneous burns, a new method was devised. A window at perigee and apogee was determined to be ±5° of true anomaly where the thrusters would be activated. Once the spacecraft exited that window, the thrusters would be deactivated. With this method, the orbit of the spacecraft could be raised and circularized repeatedly until fuel was depleted. A diagram of this approach is displayed in Figure 7.

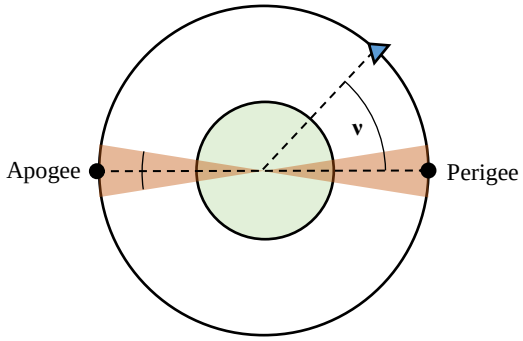

Figure 7: Thruster Activation Regions

Results using this method with the different configurations is displayed below in Table 5.

Table 5: Chemical Only - Apogee / Perigee Orbit Raising

Size	ΔV (km/s)	Altitude Gain (km)	Maneuver Time (hrs)
6U	0.88	1795	12.4
12U	1.08	2286	18.89
27U	.947	2034	40.76

When comparing these values to those in the Tsiolkovsky rocket equation, a more accurate representation of the delta V capability emerges, as shown in Table 6.

Table 6: Orbit Raising DeltaV Comparison

Size	ΔV (km/s)	ΔV (Rocket Eqn)	% Difference
6U	0.88	0.830	5.65%
12U	1.08	0.983	8.98%
27U	.947	0.716	24.4%

C. Orbital Plane Change

The logic behind the orbital plane change is simple and determines the necessary direction of thrust to enact the plane change. Once the targeted inclination is determined, the necessary final velocity vector can be determined at both apogee and perigee. Using vector subtraction, detailed in Figure 8, the necessary thrust vector can be determined and utilized for the upcoming burns.

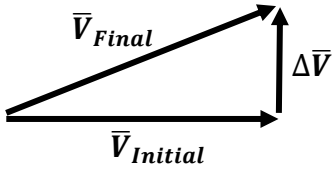

$$\Delta\overline{V} = \overline{V}_{Final} - \overline{V}_{Initial}$$

Figure 8: Plane Change Vector Geometry

The thrust direction needed for inclination change is recalculated at every pass of apogee and perigee, ensuring that the burns are conducted efficiently. Using this methodology with a target inclination of 20 degrees, an inclination change of ~2.5 degrees was reached. This initially seemed to be low value, but after validation, it appears to be within the correct order of magnitude when compared to the results of Equation 18.

$$\Delta i = 2\,sin^{-1}(\frac{\Delta V}{2V}) \tag{18}$$

The choice of target inclination for the final orbit (which determines $\overline{\mathbf{V}}_{\mathbf{Final}}$) is non-trivial and as such it is necessary to determine how the final inclination will vary as a result. A quick study was conducted to determine said impact and was performed by iterating the target inclination from 1 to 20 degrees and analyzing the output. Results can be seen in Figure 9 and Figure 10.

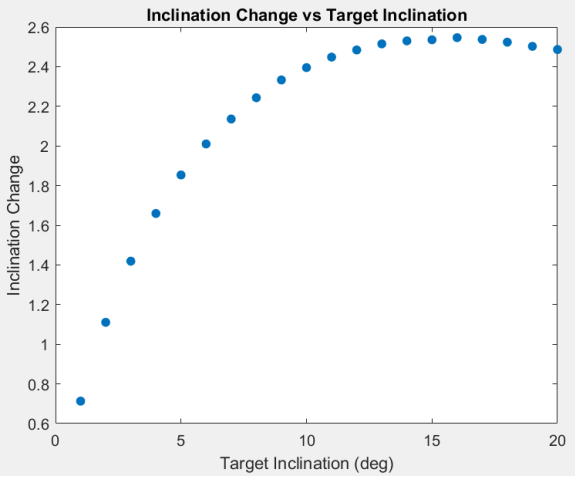

Figure 9: Inclination Change vs Targeted Inclination

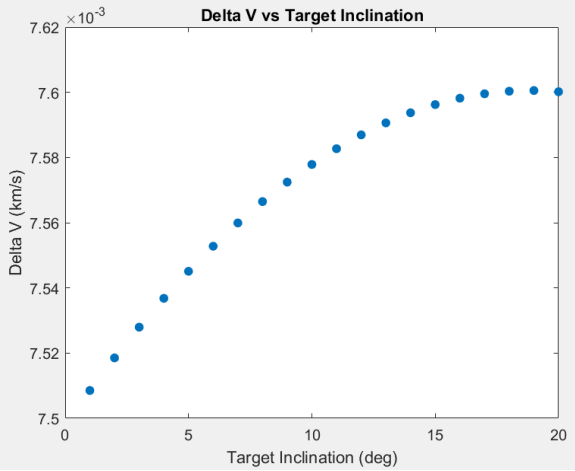

Figure 10: Delta V vs Targeted Inclination

The selection of the target inclination has a non-negligible impact on the final achieved orbital inclination. From Figure 9 it can be seen that a targeted inclination of 15 degrees will maximize the inclination change for this instance. This holds true for 6U, 12U and 27U spacecraft variants. It seems counter-intuitive that a targeted inclination much higher than the expected ~2.5 degree inclination would yield the maximum inclination change. This could likely be correlated to the sizing of the inclination window or be due to a multitude of other factors and could be explored more in depth during future development of the simulation framework.

D. Thruster Activation Window Sizing

As development progressed, the importance of the size of the thruster activation window was realized. As such, it was important to conduct a study to determine the optimal sizing of the window and how that sizing cascaded into the vehicle dynamics for both altitude raising and plane change missions. This was determined by iterating through various window sizes and analyzing how the performance outputs were impacted. Runs were conducted using window sizes ranging from 1 to 20 degrees and the primary outputs observed were ΔV and Eccentricity change. Plots of the results are shown below in Figure 11 and Figure 12.

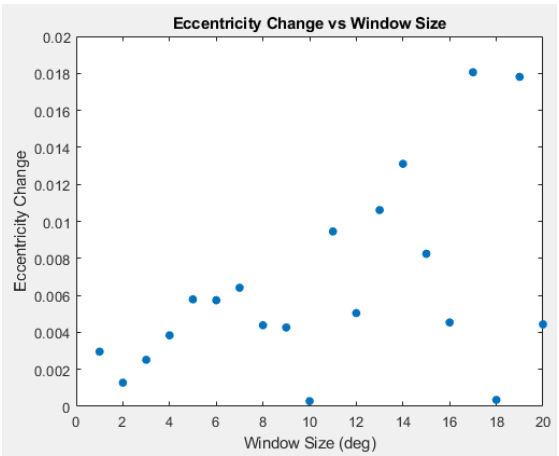

Figure 11: Eccentricity Change vs Window Sizing

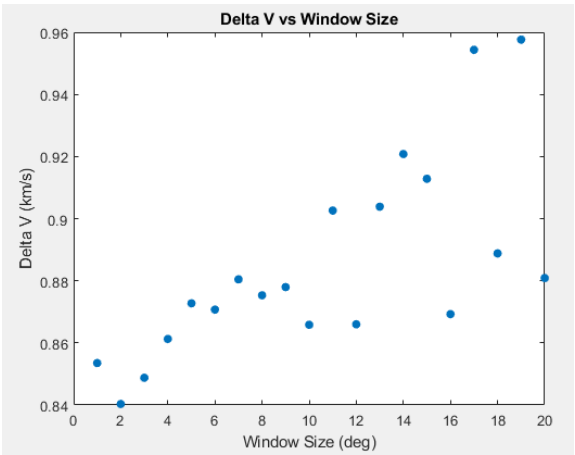

Figure 12: Delta V vs Window Sizing

In the cases of orbit raising, there is a direct correlation between the ΔV and final eccentricity in relation to the sizing of the activation window. The narrower the activation window, the more circularized the orbit, but the lower the final ΔV. In the case of the larger activation window, the increased ΔV is likely due to less of the energy being directed into the circularization of the orbit. The variance between the points, including the outliers at window sizes 10 and 18 in Figure 11 could not be immediately attributed to any specific cause and should be explored further.

Additionally, it was needed to see if the size of the activation window would impact the Orbital Place change capability. This was done using the same iterative approach, changing the window size from 1 to 20 degrees.

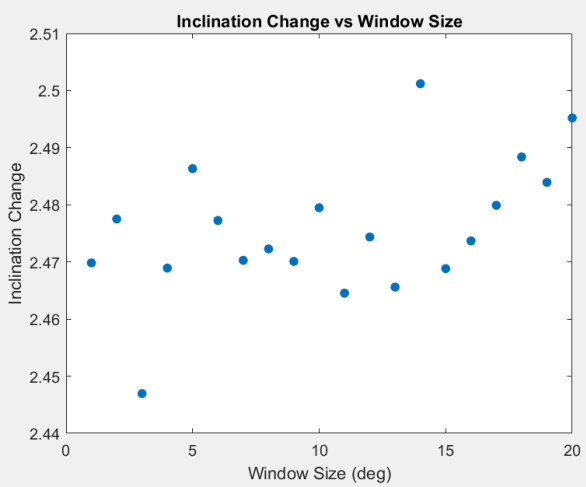

Figure 13: Inclination Change vs Window Size

From Figure 13, it can be seen that there is no obvious correlation between the window sizing and the final achieved inclination. This holds true for all spacecraft sizes observed.

E. 90-10 Fuel Distribution Study

The primary benefit of the Spectre propulsion system is the ability to switch between propulsion sub-systems as needed. As such, analyses focusing on the capabilities of the system while utilizing solely one propulsion method fail to capture the primary capability of the system. As such, further work was needed to capture a realistic representation of the spacecraft. Initial systems have the propellant budgeted between the two modes, with 90% for the chemical and 10% for the electrospray. Using this distribution, the performance statistics shown in Table 7 were established.

Table 7: 90-10 Performance Distribution

Size	ΔV (km/s)	Altitude Gain (km)	Maneuver Time (hrs)
6U	0.757	1530.6	47.9
12U	0.891	1877.2	65.8
27U	0.645	1295.3	157.5

Despite the massive reduction in fuel dedicated to the electrospray system, the time needed to exhaust the supply is still incredibly lengthy. In run detailed in Figure 14, the supply of chemical propellant was exhausted rather quickly, after which the spacecraft switched over to the electrospray thrusters, which conducted orbit raising at

Apogee and Perigee over the next ~1300 hours (~2 months). After this period of time, only 1.5% of the electrosprays allocated fuel had been burned.

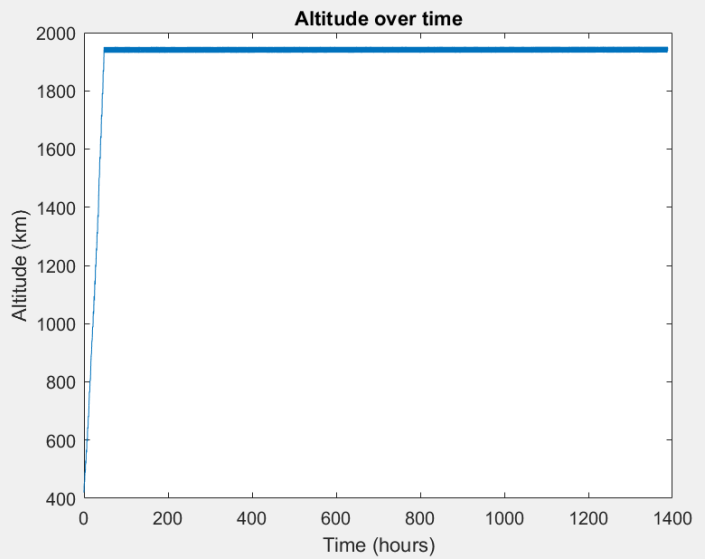

Figure 14: 90-10 Distribution Altitude Gain

The extensive timeframe encountered begins to allude to a weakness in the simulator, namely that in order to accurately model orbit raising of such a low thrust system operating at infrequent intervals, either more computational power is needed or a more efficient coding framework is needed (likely C++ or Python).

F. Lunar Orbit Excursions

The use of Small Satellites for areas outside of Low Earth Orbit has been an area of increasing development in recent years, especially with the aerospace communities increased interest in the Moon and NASA's creation of the Artemis and HLS programs. Given these developments, the author felt it would be important to characterize the vehicles performance in that domain. For the lunar excursion, the problem assumed a 2-Body problem as long as the craft remained inside the Moon's sphere of influence. This assumption greatly simplified the development of this excursion, as the implementation of the 3-Body problem would have been a non-trivial. Additionally, the spacecraft is already assumed to be in a 50 km, circular lunar orbit. Given NASA's use of Orion to deploy currently scheduled small-sat missions, as well as the development of space tugs capable to lunar injection, this is not an extreme assumption to make.

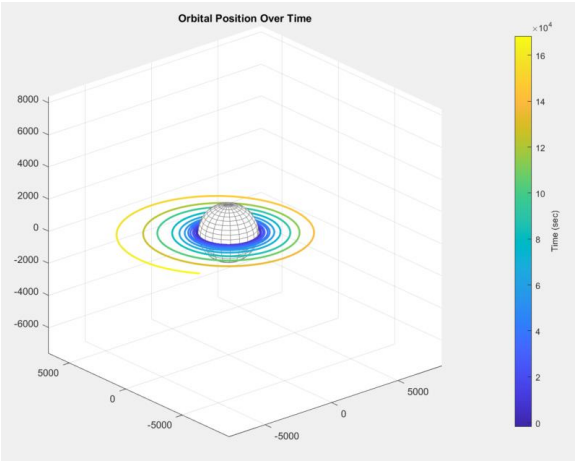

Figure 15: Lunar Orbit Raising Maneuver

Table 8: Lunar Orbit Maneuverability Summary

Size	ΔV (km/s)	Altitude Gain (km)	Maneuver Time (hrs)	Inclination Change (deg)
6U	0.878	4451.5	18.9	10.6
12U	1.01	6961.6	36.2	12.3
27U	0.648	2928.0	46.4	9.25

In comparing the values in Figure 15 and Table 8, it can be seen that the system has significantly more maneuverability while in orbit due to the reduced gravity. This is true of any craft in lunar orbit, but it is important to characterize capability in that ever developing domain.

V. Conclusions

With this simulation, a reliable framework has been established for the continued design and characterization of spacecraft systems. While current capabilities focus on establishing baselines for propulsion systems and planning orbital maneuvers, there still much more that can be done to characterize the Spectre spacecraft, including analyzing the vehicles station-keeping capabilities and looking at optimized low thrust trajectories. In addition, each of the 4 electrospray thrusters has independent capability, offering a complex attitude control problem waiting to be explored. There is also the need to add in complexity to the gravitational model, injecting perturbations to disturb the craft, allowing for tuning and testing of onboard systems. Additionally, various sections of the simulation could use optimization or streamlining to allow for more modularity and testing of craft with differing configurations. Porting the simulation over to another, more efficient programming language to allow for more powerful capability.

Acknowledgments

Firstly, I would like to thank the Lunar Flashlight and Spectre teams for their assistance throughout this project (as well as my entire graduate experience here at the GT SSDL). Special thanks goes out to Brandon Colón, whose technical insight and support have been invaluable during the effort. Finally, I wish to thank Dr. Glenn Lightsey for the opportunity to be involved in the best lab I have experienced throughout my collegiate career. The experience has truly been one of a lifetime and I will be forever grateful for the chance to study under and work alongside a group of incredibly qualified faculty and peers.

References

[1] Bate, Roger R., Mueller, Donald D. and White, Jerry E. Fundamentals of Astrodynamics. New York: Dover Publications, 1971.

[2] Spectre Table-top Review, NASA Marshall Spaceflight Center, July 30th, 2020

[3] Huggins, Grayson, and Dr E Glenn Lightsey. "Development of a Cubesat-Scale Green Monopropellant Propulsion System for NASA's Lunar Flashlight Mission," n.d., 22.

[4] Little, Bryan, and Manish Jugroot. "Bimodal Propulsion System for Small Spacecraft: Design, Fabrication, and Performance Characterization." Journal of Spacecraft and Rockets 57, no. 4 (July 2020): 707–19. https://doi.org/10.2514/1.A34555.